Journal of Polymers and the Environment
https://doi.org/10.1007/s10924-024-03314-5

ORIGINAL PAPER

Effect of Compatibilizers on the Physico-mechanical Properties of a Poly(Lactic Acid)/ Poly(Butylene Adipate-co-terephthalate) Matrix with Rice Straw Micro-particle Fillers

Dylan Jubinville[1] · Mohammed Awad[1,2] · Hyung-Sool Lee[3,4] · Tizazu H. Mekonnen[1]

Accepted: 1 May 2024

Abstract
This study explores the blending of poly(lactic acid) (PLA) and poly(butylene adipate-co-terephthalate) (PBAT) with rice straw micro-particles (10 to 30 wt%, ≤ 250 µm) to create biocomposites using a kinetic mixer. It examines the effects of chain extender (J) and maleic anhydride (MA) as compatibilizers on material properties. Biocomposites underwent 500 h accelerated weathering to simulate environmental conditions, with analysis via Fourier-transform infrared spectroscopy (FTIR), mechanical testing, dynamic mechanical analyses (DMA), and rheological evaluations. Results indicate that the chain extender's superior performance over MA, generating 6% insoluble content compared to 1% with MA. Scanning electron microscopy (SEM) revealed reduced interfacial voids in biocomposites treated with compatibilizers. The addition of the rice straw was found to increase the tensile modulus from 2.3 to 3.4 indicating a 43% increase after 40 wt% rice particles; all the while reducing the tensile strength and ductility. Post-weathering, *Joncryl*® treated samples retained properties better than MA-treated ones, showing enhanced crosslinking and less decline in tensile strength (10–19% reduction for J vs. 27–30% for MA). Compatibilizers, especially the chain extender, play a crucial role in strengthening PLA and PBAT biocomposites, particularly under accelerated weathering.

Keywords Rice straw · *Joncryl*® · Poly(lactic acid) · Poly(butylene adipate-co-terephthalate) · Maleation · Micro-particles

Introduction

Rice, a major global food crop, yields approximately 523.9 million tonnes (MT) annually, with a global rice usage being 522.0 MT in 2023 which has seen a slight decline due to increasing domestic and internation prices limiting its use for animal feed [1]. While rice straw and husk are under-utilized in composite applications, their collection poses a challenge. Current applications include animal feed, fuel, bio-ethanol, and organic synthesis [2, 3]. Rice straw, comprising lignocellulosic components presents challenges due to its high ash content 8 to 38%, limiting its use in animal feed when compared to the holo-cellulose (51 to 74%) and lignin (5 to 24%) [4]. Incineration, the prevalent disposal method, contributes to greenhouse gas emissions and poses environmental risks. Furthermore, uncollected rice straw may harbor rice diseases as it degrades slowly and also cause physiological damage to the cultivating land, particularly to paddy soil [4]. Utilizing rice straw in thermoplastic composites could enhance material properties and offset costs. Research predominantly focuses on husk or straw fiber, with limited exploration of particulate rice straw usage. The use of particulate fillers provides a more straightforward process, when compared to oriented fibres or pre-peg operations, as well particulate reinforcement provides a more

✉ Tizazu H. Mekonnen
tmekonnen@uwaterloo.ca

1 Department of Chemical Engineering, Institute of Polymer Research, Waterloo Institute of Nanotechnology, University of Waterloo, Waterloo N2L 3G1, Canada

2 School of Engineering, Samarkand Internation University of Technology, Samarkand, Uzbekistan

3 Department of Environmental and Climate Technology, Korea Institute of Energy Technology, Yuseong-gu, Republic of Korea

4 Greeneple Inc, Seoul, Republic of Korea

Published online: 03 July 2024

Table 1 Sample guide and breakdown for each specimen by wt%

	PLA (wt%)	PBAT (wt%)	Rice (wt%)	MA (wt%)	J (wt%)
PLA: PBAT	80	20	0	0	0
PLA: PBAT + M	76	19		5	0
PLA: PBAT + J	79	20		0	1
MR10	68	17	10	5	0
MR20	60	15	20		
MR30	52	13	30		
JR10	71	18	10	0	1
JR20	63	16	20		
JR30	55	14	30		

localized isotropic response to applied stresses. The most common application for rice straw is as a low-cost filler for particle boards. This is a result of particulate reinforcement providing a higher degree of global heterogeneity (with good dispersion) as opposed to the anisotropic response from oriented or woven fibres [5]. For composite compounding, the most common thermoplastic resin types are low- and high-density poly(ethylene) (LDPE) and (HDPE) [3, 6], poly(lactic acid) (PLA) [7–9], and poly(propylene) (PP) with the most common polymer being PP [10–12].

Poly(lactic acid) (PLA), a renewable thermoplastic, is known for its eco-friendly properties but faces challenges like brittleness and slow biodegradation [13–15]. However, Due to PLA's glass transition temperature (T_G), above room temperature (~70 °C) [15], the composting conditions for PLA are limited making biodegradation with soil slow-acting and to a low degree of success without additional assistance [14]. Additionally, the biggest industry for PLA is in packaging and more recently in 3D printing [14]. Blending PLA with poly(butylene adipate-co-terephthalate) (PBAT) and other ductile polymers, improves its overall toughness and energy dampening. Compatibilization agents, such as maleic anhydride and polyfunctional chain extenders, enhance PLA-PBAT blend compatibility. In literature, other bio-based and agriculture byproducts that have been used with PLA and PBAT may include, mango seed waste, almond shells, hazelnut shells but few papers examine specifically the blending and compounding of a PLA: PBAT matrix with micro-rice straw powder [16–18].

Therefore, this study aims to create a sustainable route for rice straw utilization within polymer composites, addressing environmental concerns linked to incineration. It also explores PLA-PBAT blend compatibilization using agents like chain extenders and maleic anhydride. Additionally, the research investigates the durability of the composites in simulated outdoor conditions through accelerated weathering tests.

Experimental Section

Compounding Materials

The poly(lactic acid) (PLA) utilized in this study (Total Corbion, Luminy LX 175) demonstrated a melt flow index (MFI) and density of 6 g/10 mins (at 210 °C /2.16 kg) and 1.26 g/cm^3, respectively. The PBAT (T&T Industry Group) had an MFI of 5 g/10 mins (at 190 °C/ 2.16 kg) and a density of 1.24 g/cm^3. Maleic anhydride, compatibilization agent, and dicumyl peroxide (DCP), a radical initiator, were both procured from Sigma without prior modification. Joncryl® ADR-4468 (J) in pellet form was generously provided by BASF (NJ, USA) without additional treatment. Unrefined rice straw (RS) from the Korea Institute of Energy Technology (KENTECH) underwent grinding with an IKA MF10 grinder (IKA Works, Inc., Wilmington, NC, USA) set to 4000 rpm and feed through a 3 mm sieve. The resulting particles, were then furthered sieved to ≤250 µm, ensured uniformity and minimized inherent failures like cracks. Before processing and characterization, the rice straw microparticles were dried to achieve a moisture content of 1.3 ± 0.1%.

Composite Compounding

Melt Blending and Composite Compounding

The blends and their composites compositions, shown in Table 1, were prepared by using a HAAKE Rheomix 3000 batch mixer (Thermo-Fisher Scientific Inc., Waltham, MA, USA) at a mixing temperature and screw speed of 180 °C and 100 rpm, respectively. Although the mixer was set to 180 °C, the temperature of the polymer melt ranged from 190 to 200 °C depending on the level of filler content (10 to 40 wt%) due to the increased friction and pressure. Resultant samples were then ground, using a laboratory Wiley mill, to obtain smaller granules that are suitable for injection and compression moulding purposes.

In-situ Maleation Reaction Extrusion and Joncryl® Usage

Concerning the creation of compatibilized blends and composites, dicumyl peroxide (DCP) was incorporated in-situ into the polymer melt blend at 180 °C, once the torque had stabilized in the batch mixer after approximately 5 min of mixing. The addition of 0.1 wt% of peroxide was mixed for 0.5 min before introducing maleic anhydride (MA) at 5 wt%, which was also mixed for 30 s. When blending the (80:20) blend with 1 wt% of a compatibilizing agent (J), the same process was followed. Once the (80:20) blend reached equilibrium torque, the *Joncryl*® was added and allowed to mix for 0.5 min. It is noteworthy that preliminary results indicated that 5 wt% of *Joncryl*® supplied the system with excessive molecular weight, leading to overly tough and non-processable material under the same processing parameters for all specimens.

For the composites, rice straw microparticles were introduced as a final processing step and mixed until a stabilized torque was achieved, ensuring the mixing temperature did not exceed 200 °C. The compatibilized 80:20 PLA: PBAT blends and composites for characterization underwent a process of grinding, washing (acetone washing, and centrifugation at 4500 revolutions per minute for five minutes, repeated three times), followed by drying in a vacuum oven to eliminate residual MA molecules for further characterizations.

Injection and Compression Molding

The injection molding machine employed, namely the HAAKE Mini-Jet Pro, operated at a single temperature point of 200 °C with a mold temperature of 70 °C. This temperature was utilized to melt the polymer test samples, which were subsequently injected under high air pressure (750 bar) and maintained for three seconds. This process aimed to yield tensile specimens (Type V) and parallel plate discs for rheology, ensuring a minimum of five replicate samples. To produce thin polymer films (with dimensions L×W×T of 76 × 75 × 0.2 mm³), a Carver compression machine was utilized. In this procedure, polymer granules were positioned between two heated plates set at 200 °C and subjected to incremental pressure, reaching six metric tons, over a three-minute duration.

Characterization Techniques

Attenuated Total Reflection– Fourier Transform Infrared Spectroscopy (ATR-FTIR)

Nicolet 6700 model (Thermo-Fisher Scientific Inc., Waltham, MA, USA) with an attached high-temperature GladiATR accessory (PIKE Technologies, Fitchburg, WI, USA) were used to investigate the FTIR spectra of the test samples. Thin films (thickness of 0.2 mm) of each test sample were compressed using a Craver press for 3 min under 6 metric tons of force. Moreover, the absorption mode in the 400 to 4000 cm^{-1} range with a resolution of 4 cm^{-1} at 64 scans was applied.

Gel-Fractionation (Soxhlet Extraction)

Gel content measurement (ASTM D2765) was employed to quantify the amount of crosslinking that had occurred, and to determine the efficacy of the two different compatibilizing systems. Firstly, all samples were weighed to a constant initial weight with an analytical balance; following which, the samples were placed in a Soxhlet extraction set-up with boiling chloroform for a period of 6 h. The samples were placed into a vacuum oven at 50 °C overnight to remove any residual chloroform from the surface of the extractables. For the case of the composites, the final weight was offset by the amount of the filler (e.g. 30%) to compensate of the insoluble filler component. The final weight of the gel content percentage was calculated as an average, using Eq. 1, for each tested sample.

$$\%Gel = \left(\frac{W_F}{W_I}\right) * 100 \tag{1}$$

Where W_I is the initial weight of the prepared samples in grams, W_F is the final weight of the samples after extraction process.

Rotational Viscosity

ASTM D4440 standard was followed to study the rheology of the PLA: PBAT blends and their rice straw composites utilizing a HAAKE MARS III rheometer equipped with parallel-plate geometries. Using a diameter thickness of 25 and 2.5 mm, respectively, for the samples and a frequency sweep of 0.1 to 100 rad/s at 200 °C under a constant strain of 0.01% and a plate gap of 1.0 mm. Additionally, the Cross model (Eq. 2) was used to model fit the complex viscosity data in order to obtain zero-shear viscosity information.

$$\eta = \left(\frac{\eta_0}{(1 + (\tau_0\gamma)^m)}\right) \tag{2}$$

Dynamic Mechanical Analysis (DMA)

The glass transition and modulus data were obtained using a dynamic mechanical analyzer (DMA Q800 from thermal

analysis (TA) Instruments by using a thin film of 0.3 mm thickness. Tension clamp in multi-frequency-strain mode with an applied frequency of 1.0 Hz and strain, preload or static force, and force tracker of 0.01% (within the LVR), 0.01 N, and 0.125%, respectively. The experiments were preformed from (-)50 to (+)90 °C with a rate of 3 °C/min.

Thermal Gravimetric Analysis (TGA)

TGA was used to observe the stability of the rice straw, when placed in a thermal environment, to find its onset to degradation as well as to gain insight into its composition (e.g. cellulose, hemicellulose, lignin, ash content). A TGA Q500 (TA Instruments, New Castle, DE, USA) was used in this investigation. The test consisted of a sample weighing ~ 10 mg and a temperature ramp of 10 K/min was applied from 30 to 600 °C in a nitrogen environment with a flow rate of 40 mL/min.

Mechanical Properties

The tensile test on the injection-molded specimens was carried out utilizing a Shimadzu– AGS X tensile testing unit, which was equipped with a 10 kN load cell (Shimadzu Corp., Kyoto, Japan). The test was performed at a consistent crosshead speed of 10 mm/min for all samples, adhering to the ASTM D638 Type V standard, with a gauge length of 25 mm. For each sample, five tensile bars were tested in order to generate testing statistics and the material's repeatability. For the measurement of notched Izod impact properties, a Testing Machines Inc. TMI Monitor Impact Tester was employed, and the test was conducted in accordance with ASTM D256. Prior to the impact testing, a 2 mm deep notch was introduced into the test specimens.

Environmental-scanning Electron Microscopy (E-SEM)

All specimen's facture morphology of the tensile (tested) specimens were surveyed with an environmental scanning electron microscopy (Oxford Instruments Quanta FEG 250) to avoid having to surface coat the samples.

QUV Accelerated Weatherability

A QUV weatherometer was used to simulate accelerated artificial environmental damage mimicking sunlight (UV), heat (temperature) as well as rain and/or dew (moisture absorption) following ISO 4892-3 exposure mode 1 [19, 20]. As such, the specimens were cycled through periods of UV exposure followed by periods of condensation without radiation effect all while under controlled temperature. Tensile dog bone samples were mounted to the supplied aluminum fixtures and were subjected to accelerated UV aging by exposure to 340 nm fluorescent UV lamps (UV-B lamps). The following procedure for the weatherometer was as follows [19, 20]: 8 h of UV exposure (dry) at a temperature of 60 °C, 4 h of condensation exposure of 80% at a temperature of 40 °C without radiation and Repeat steps every 12 h to a maximum of 500 h. After the samples had been removed from the weatherometer, the weathered dog bone samples were subject to tensile properties.

Statistical Analysis (ANOVA)

A one-way unstacked analysis of variance (ANOVA) test was conducted to evaluate any significant difference between the means between the different filler amount in addition to comparing the effectiveness of the compatibilizers. The difference in the replicate's means was considered significant at level of 5% ($p < 0.05$).

Results and Discussion

Chemical Structure Investigation

The comprehensive ATR-FTIR analysis of the rice straw, blends, and composites is presented in Fig. 1. In Fig. 1(**a**) and (**b**), distinct peaks corresponding to PLA and PBAT can be discerned. The primary PLA peaks are associated with OH twisting and C = O stretching, occurring at 1457 and 1733 cm^{-1}, respectively [21]. Meanwhile, the PBAT peaks are observed at 726 cm^{-1}, 871 cm^{-1}, 1710 cm^{-1}, and 2800 to 3000 cm^{-1} attributed to CH_2 stretching, benzene ring vibrations, C = O stretching, and the deformation of terminal C-H groups, respectively [22–24]. A zoomed in version of the spectra (400 to 1200 cm^{-1}) may be found in the supporting information file as Figure S1.

For both the chain extender and MA compatibilized specimens, the noteworthy development was the emergence of a new shoulder region or peak splitting in the polyester peak at ~ 1715 to 1755 cm^{-1}. This phenomenon suggests an enhanced interaction among the constituents, possible through processes, such as transesterification, hydrogen bonding, and entanglements. In the case of MA compatibilization depicted in Fig. 1(a), the new peak can be attributed to ester-carbonyl stretching vibrations originating from the grafted functionalized MA groups integrated onto the backbones of PLA and PBAT, as well as interacting with the hydroxyl groups present on the rice straw surface [21, 25]. Furthermore, at ~ 750 cm^{-1} the signal intensity is observed to increase in both cases, likely due to the increased presence of the aromatic rings in the systems. Additionally, the appearance of a new peak at 728 cm^{-1} signifies interaction

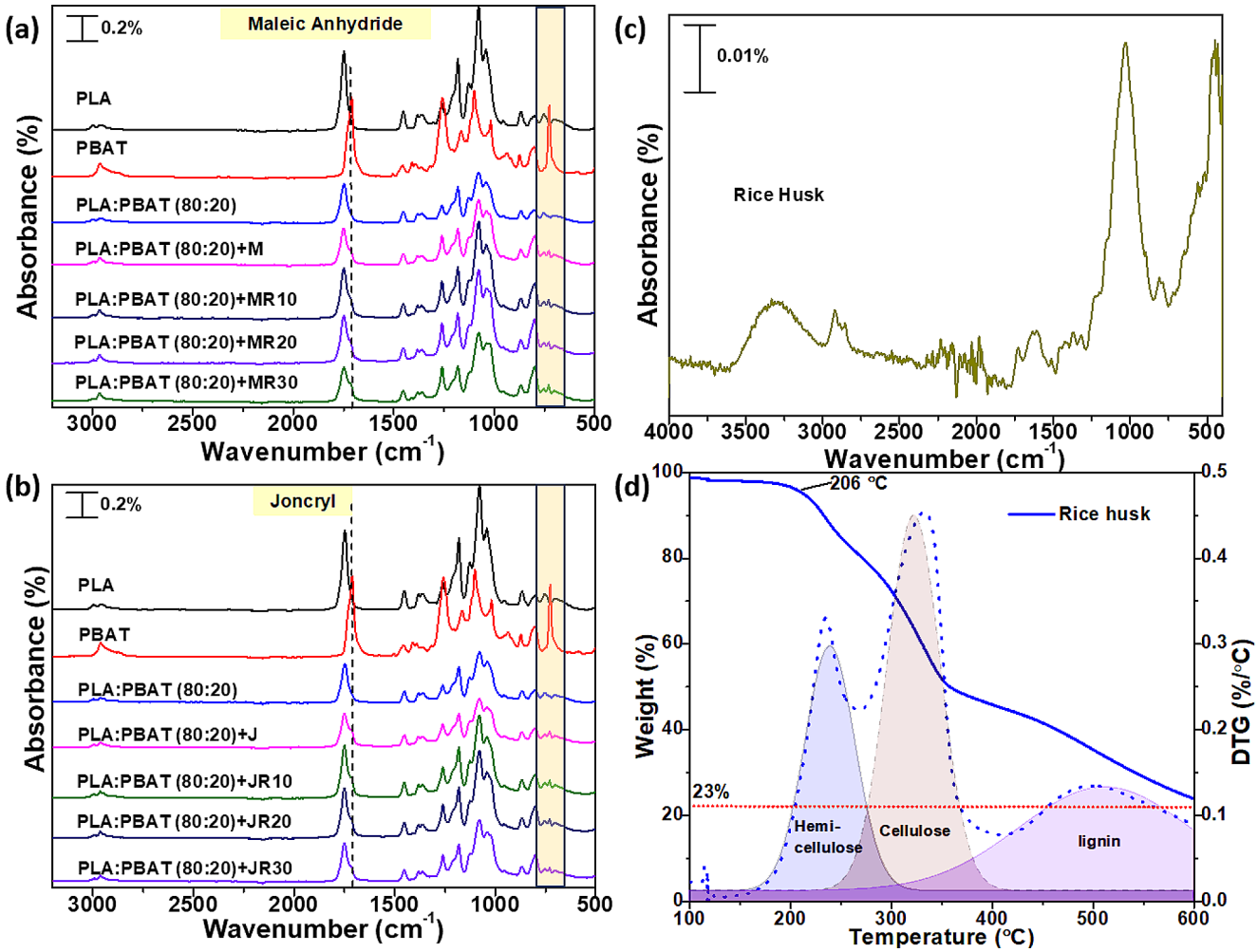

Fig. 1 (**a**) Full ATR-FTIR spectra (500 to 4000 cm^{-1}) for the MA containing samples; (**b**) Full ATR-FTIR spectra (500 to 4000 cm^{-1}) for the J containing samples; (**c**) Full ATR-FTIR spectra (500 to 4000 cm^{-1}) for the rice straw microparticles; and (**d**) TGA weight degradation and weight derivative curves for the rice straw microparticles

among the functional groups of all constituents. Figure 1(c) and (d) show typical FTIR spectra for the ground rice straw powder along with TGA evaluation to determine holo-cellulose to lignin components. In Fig. 1(c), prominent peaks are observed at 447 and 1030 cm^{-1}, with additional notable bands at 3313 and 2915 to 2850 cm^{-1} attributed to silicon groups (e.g., inorganic components on the biomass filler), hydroxyl groups, and aromatic components from the lignin fraction [22, 23]. Following these intense signals, several medium to weak intensity bands at 1980, 1700, 1410, and 850 cm^{-1} can be identified, corresponding to alkanes and alkenes, aromatic stretching, and ether groups [26, 27]. In Fig. 1(d), the thermal degradation of rice straw is depicted, commencing around 200 °C and extending beyond 600 °C, yielding a residue of 23%. The analysis reveals that cellulose is the primary constituent, initiating degradation at ~250 °C, followed by hemi-cellulose at 200 °C, and lignin, which begins to degrade at ~400 °C [26]. Given that cellulose and hemi-cellulose constitute the major components of biomass fillers, their abundance in holo-cellulose components facilitates more efficient modification and grafting reactions compared to targeting the lignin component.

The extent of crosslinking or formation of 3D networks, facilitated by polymer compatibilization, was assessed through gel fractionation tests, as depicted in Fig. 2(a). Initially, the base blend (80:20) was observed to completely dissolve in boiling chloroform. Since the blend does not present any reaction, the crystalline structures of each component can easily be disrupted by the solvent leading to swelling and dissolution [28, 29]. Upon introducing a compatibilizing agent, the gel content in the blends increased to varying degrees. In the compatibilized blends, the *Joncryl*® compatibilizer exhibited higher efficacy and functionality, resulting in a greater degree of crosslinking (~6%) compared to the maleated blend, which only achieved a~1% gel content, as illustrated in Fig. 2(b. This trend continued,

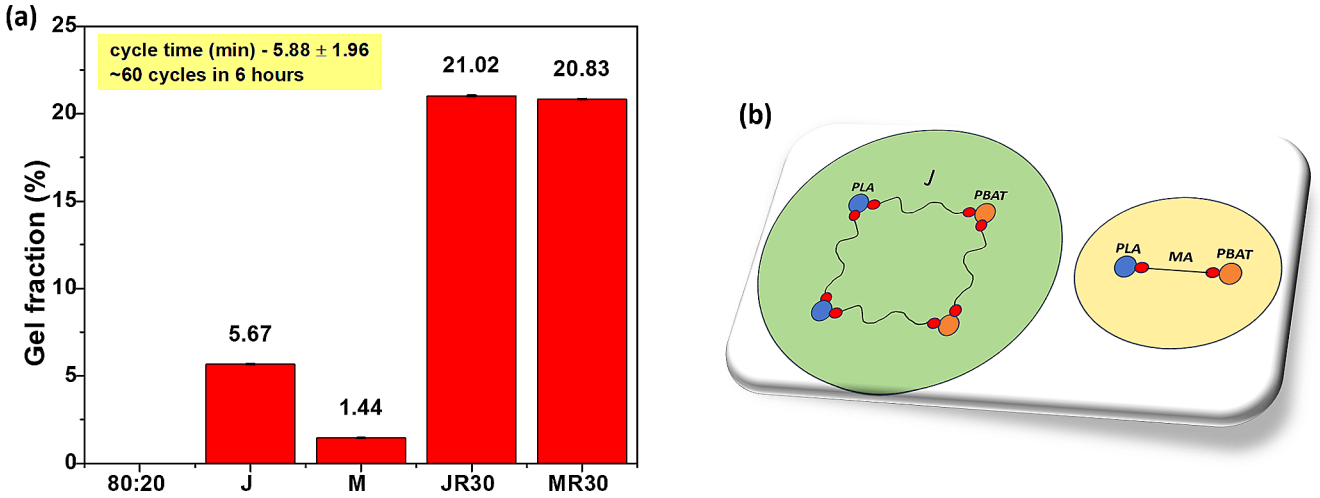

Fig. 2 (**a**) Gel-fractionation results after 24 h of Soxhlet extraction; (**b**) Schematic representation of bonding and crosslinking potential of the two compatibilizing agents (e.g. J and MA)

with composites demonstrating an even higher production of gel content due to the formation of new bonds between the compatibilized blends and the rice filler. The *Joncryl*® compatibilized composites showed a 250% increase with a gel content of ~21%; while, the MA composite experienced a 2000% at a gel content of ~21% which would suggest that the studied compatibilizing agents have high tendency to create new bonds between the rice straw filler and the polymer components. As mentioned, it should be noted that the composite's extractable masses were offset by 30% in order to compensate for the addition of an already insoluble filler.

Thermal and Dynamic Properties

The thermal decomposition of rice straw is depicted in Fig. 1(d), revealing a mass loss curve characterized by three distinct phases indicative of dehydration, active pyrolysis, and passive pyrolysis [26]. The initial phase, involving moisture removal, occurs in the temperature range from room temperature to approximately 105 °C. The subsequent phase, active pyrolysis, transpires between 110 and 400 °C and is primarily associated with the decomposition of hemicellulose and cellulose [26]. Passive pyrolysis, extending from 110 to 900 °C, represents the principal thermal decomposition mechanism for lignin, exhibiting a slow degradation profile in the region where the hemicellulose DTG peak is located, albeit persisting at temperatures exceeding 400 °C [26]. Comparing our findings with values found in the literature, it becomes apparent that the decomposition regions for hemicellulose, cellulose, and lignin differ slightly. The established temperature ranges are typically 220 to 330 °C for hemicellulose, 300 to 440 °C for cellulose, and > 400 °C for lignin [26]. In contrast, our TGA curve indicates that hemicellulose, cellulose, and lignin decompose within the ranges of 106 to 310 °C, 244 to 405 °C, and 260 to > 600 °C, respectively. This variation can be attributed to differences in sample preparation, with smaller particle sizes resulting in increased surface area exposure, and geographical variations in the origin of the rice straw samples. From the TGA investigation, it is evident that the processing of rice straw composites should be conducted at temperatures not exceeding 205 °C to prevent the onset of thermo-oxidative degradation in the rice straw.

In the DMA investigation (Fig. 3(a)), two distinct peaks were observed, corresponding to PBAT at (-)24 ± 2.05 °C and PLA at (+)70 ± 0.57 °C. However, the noticeable separation between these peaks underscores the poor thermodynamic compatibility between these polymers. It's worth noting that the individual glass transition temperatures (T_Gs) of pure PBAT and PLA polymers were identified at (-)24 ± 2.05 °C and (+)69 ± 0.40 °C, respectively. PBAT typically exhibits a T_G closer to (-)21 ± 1.37 °C, and deviations from this value suggest an inadequate interfacial balance between the two incompatible phases, leading to a two-phase morphology, as illustrated in Fig. 5(a) [24, 30, 31]. Upon compatibilization with either J or MA, similar yet contrasting effects were observed, depending on the specific polymer. The chain extender shifted the PBAT tan δ peak towards the PLA's peak, altering it from (-)27 to (-)24 °C (a shift of 14%), with no significant change in the PLA peak. Conversely, the MA-containing blend exerted a more pronounced nucleating influence on the PLA phase, shifting its peak from (+)70 ± 0.57 to (+)59 ± 0.14 °C (a shift of ~16%), while the PBAT peak remained relatively unchanged. In the case of the composites (Fig. 3(b)), the introduction of rice straw had a nucleating effect on both the J and MA systems, with MA proving to be more effective on the PBAT component with the JR30 and MR30 having T_G's

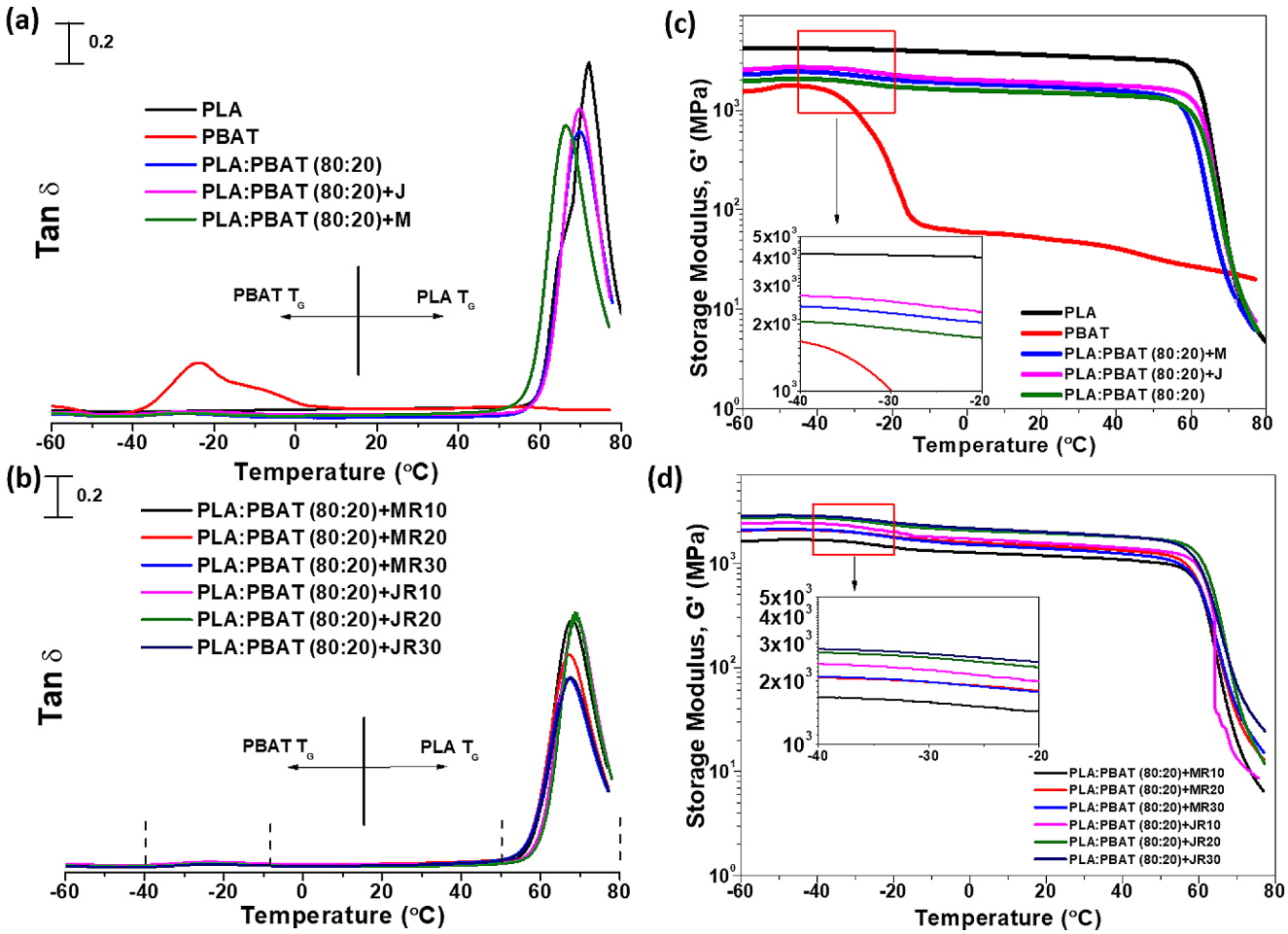

Fig. 3 (**a**) Tan δ from the DMA multi-frequency-strain mode for the blends; (**b**) Tan δ from the DMA multi-frequency-strain mode for the composites; (**c**) Storage modulus from DMA for the blends; and (**d**) Storage modulus from DMA for the composites

of 66 and 67 C which is a decrease of 5 and 4% respectively, from the baseline blend. This can be attributed to the rice straw impeding the polymer's crystallization ability, delaying its crystallization process. A zoomed version of the Tan δ graphs can be found in Figure S2 in the supporting information file.

In Fig. 3(c), the storage modulus exhibits two significant transitions, which align with the tan δ peaks, accompanied by a gradual softening of the material as the temperature varies from (-)40 to (+)80 °C. Additionally, it's noteworthy that the storage modulus increased following maleation, indicating an enhancement in material stiffness due to increased interaction/crosslinking between PLA and PBAT. Moreover, the storage modulus tends to rise further with the progressive addition of rice straw, peaking at 30 wt% rice straw, signifying an increase in material stiffness. This observation aligns well with both the rheological results (Fig. 4) and the mechanical properties in Fig. 7(a) and (b). For the *Joncryl*® modified blend and composites, the modulus experiences an even greater increase compared to MA. This can be attributed to the increase in molecular weight (MW) and crosslinking of these samples. Finally, as depicted in Fig. 3(c), the storage moduli of the blends and compatibilized blends fall between the values of the baseline polymers, further underscoring the inferior compatibility between the constituent materials. The nucleating effect and increase in modulus is a common trend found in the literature for composites filled with rice straw and other fillers such as wood flour [9, 32–34]. This is commonly attributed to the rice straw and wood flour acting as heterogenous crystallization sites however the induced nucleation is quite small in comparison to nucleating additives [33, 34].

Figure 4(a) and (b) present the complex viscosity, as well as the storage and loss moduli for all the samples. In the complex viscosity data, it was evident that the blend at 200 °C exhibits a nearly Newtonian plateau at low frequencies, transitioning to shear thinning behavior as angular frequencies increase from moderate to high. Conversely, the maleated blend displays a reduced Newtonian plateau and predominantly demonstrates shear thinning behavior across

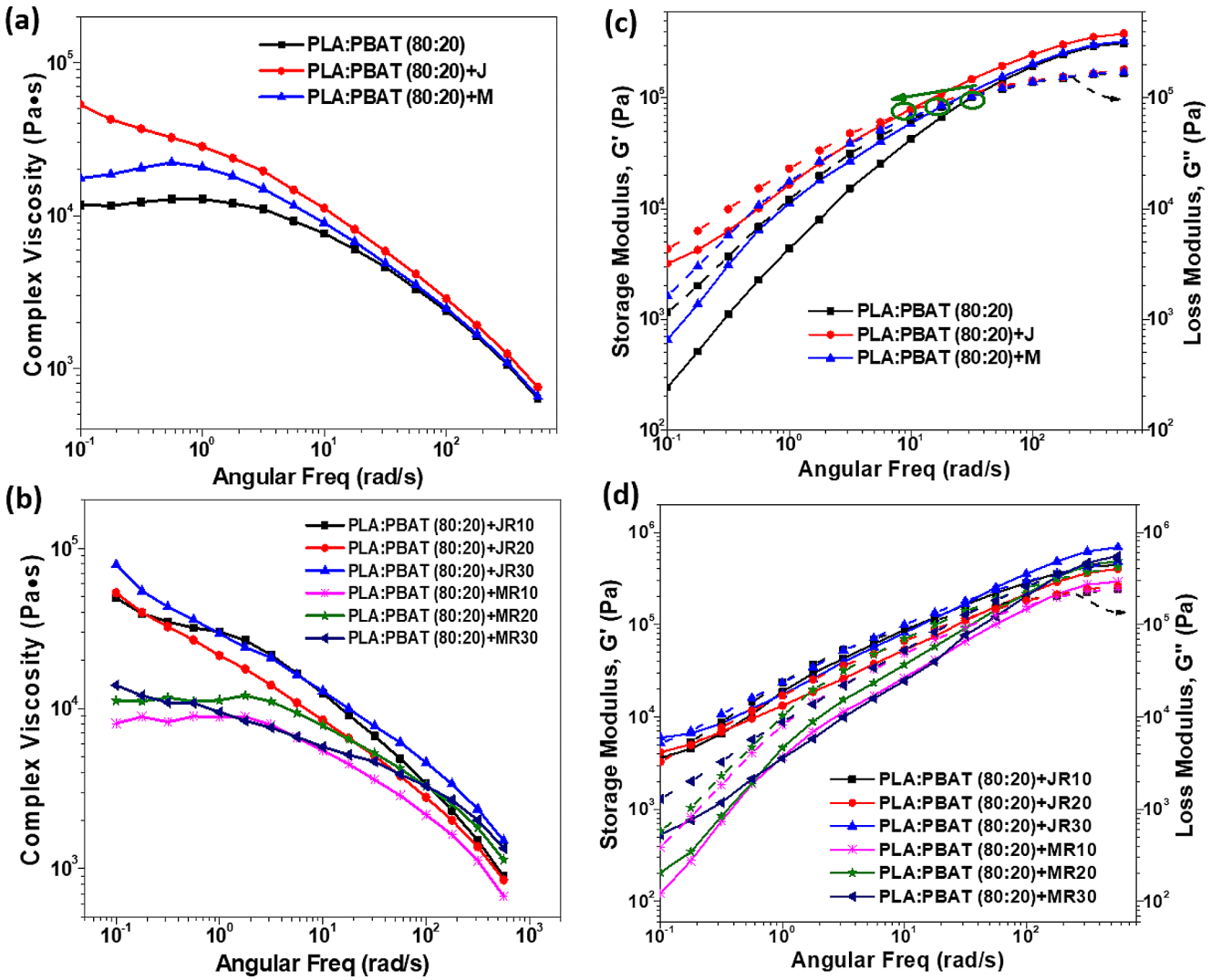

Fig. 4 (**a**) Storage and loss moduli from rotational rheology for the blends; (**b**) Storage and loss moduli from rotational rheology for the composites; (**c**) Complex viscosity from rotational rheology for the blends; and (**d**) Complex viscosity from rotational rheology for the composites

all frequencies. This transformation can be attributed to the heightened grafting and crosslinking occurring between the molecular chains of PLA and PBAT. Similar results have been found in other blending investigations that focus on compatibilizing PLA with PBAT [35]. Furthermore, the addition of rice straw particles leads to an increase in viscosity, with each subsequent addition of rice straw particles resulting in a further surge in viscosity. The highest viscosity values are observed in the MR30 and JR30 composites. Table 2 provides the zero-shear viscosity data (prior to weathering or aging), calculated by fitting the complex viscosity curve using the Cross model. These zero-shear viscosity values align with the graphical trends, increasing first due to maleation and subsequently rising with the incorporation of rice straw into the matrix.

The storage and loss moduli for the blends are presented in Fig. 4(c) and (d) while separated graphs, by there compatibilizer, can be found in the supporting information file as Figure S3. It is noticeable that the moduli increases with increasing angular frequency. At low frequencies, the loss modulus (G") is observed to be above the storage modulus (G') which indicated a visco-elastic behaviour. However, at moderate to high frequencies, the material's behaviour shifts towards composites that are dominated by their fillers, a G' surpasses G", signifying a more solid-like behaviour. Notable, the crossover modulus and frequency points exhibit a shift towards lower frequencies and moduli when compatibilized, with the chain extender compatibilized samples (Fig. 4(a)) showing the most pronounced shift. This suggest a widening of the molecular weight distribution (MWD) along with an increase in molecular weight (MW) in these cases. In contrast, the compatibilized composites follow a similar trend to the blends (Fig. 4(b)) with one exception: the crossover moduli and frequencies shifts

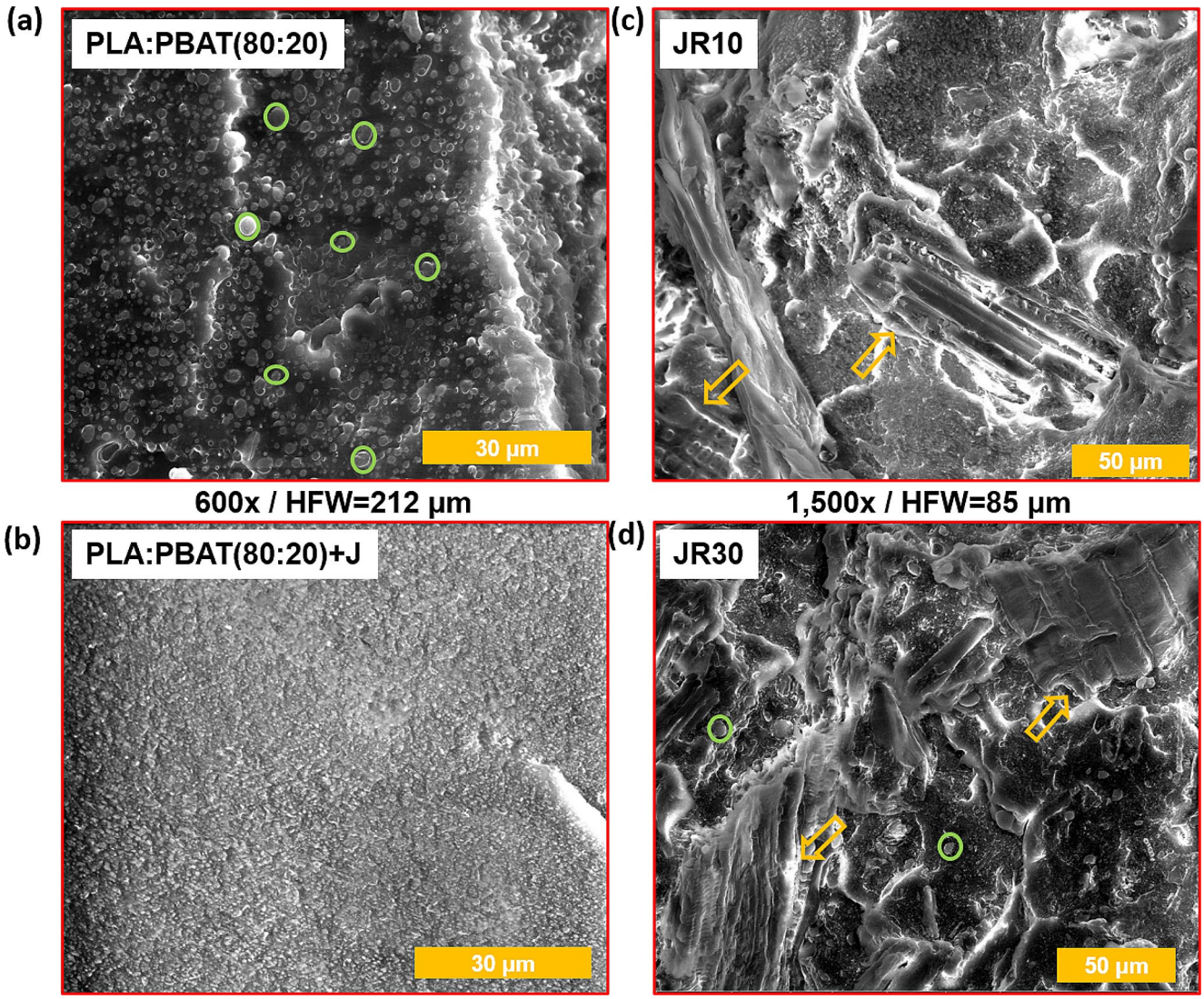

Fig. 5 SEM micrographs of the J containing specimens at 600 and 1,500x magnifications. (**a**) baseline blend of PLA: PBAT (80:20); (**b**) compatibilized blend with 1 wt% J; (**c**) J compatibilized composite with 10 wt% rice straw microparticles; and (**d**) J compatibilized composite with 30 wt% rice straw microparticles

in the opposite direction of the blends mainly the composites shifts to the right and upwards. These types of shifts crossover moduli (Pa) and frequencies (rads/s) indicates a narrowing of MWD and a reduction in MW, implying a distinct hinderance to molecular chains when the composites are being formed.

Morphology and Mechanical Properties

Analysis of the SEM micrographs of the PLA: PBAT blend reveals significant insights, as illustrated in Fig. 5(a) and Fig. 6(a). In the non-compatibilized (80:20) blend, an inconsistent morphology is evident, characterized by a distinct secondary PBAT phase in droplet form (Fig. 4(a) and Fig. 5(a)). This is attributed to the weak bonding between the polymer phases, a well-documented phenomenon in existing literature [24, 31, 36, 37] It's worth noting that these secondary PBAT droplets (see green circles in SEMs) are dispersed within the PLA matrix, with an average droplet size of 1.5 ± 0.9 µm. In contrast, the *Joncryl*® compatibilized system shows a remarkable transformation. The secondary PBAT phase is no longer discernible, and the blend surface exhibits a homogeneous morphology with minimal defects, as depicted in Fig. 5(b). Although the MA compatibilized system also demonstrates improvement over the baseline blend, slight signs of a two-phase morphology persist, further highlighting the superior efficiency of the chain extender additive, as depicted in Fig. 6(b).

Moving on to the composite systems, both compatibilizing agents prove effective in reducing interfacial boundaries

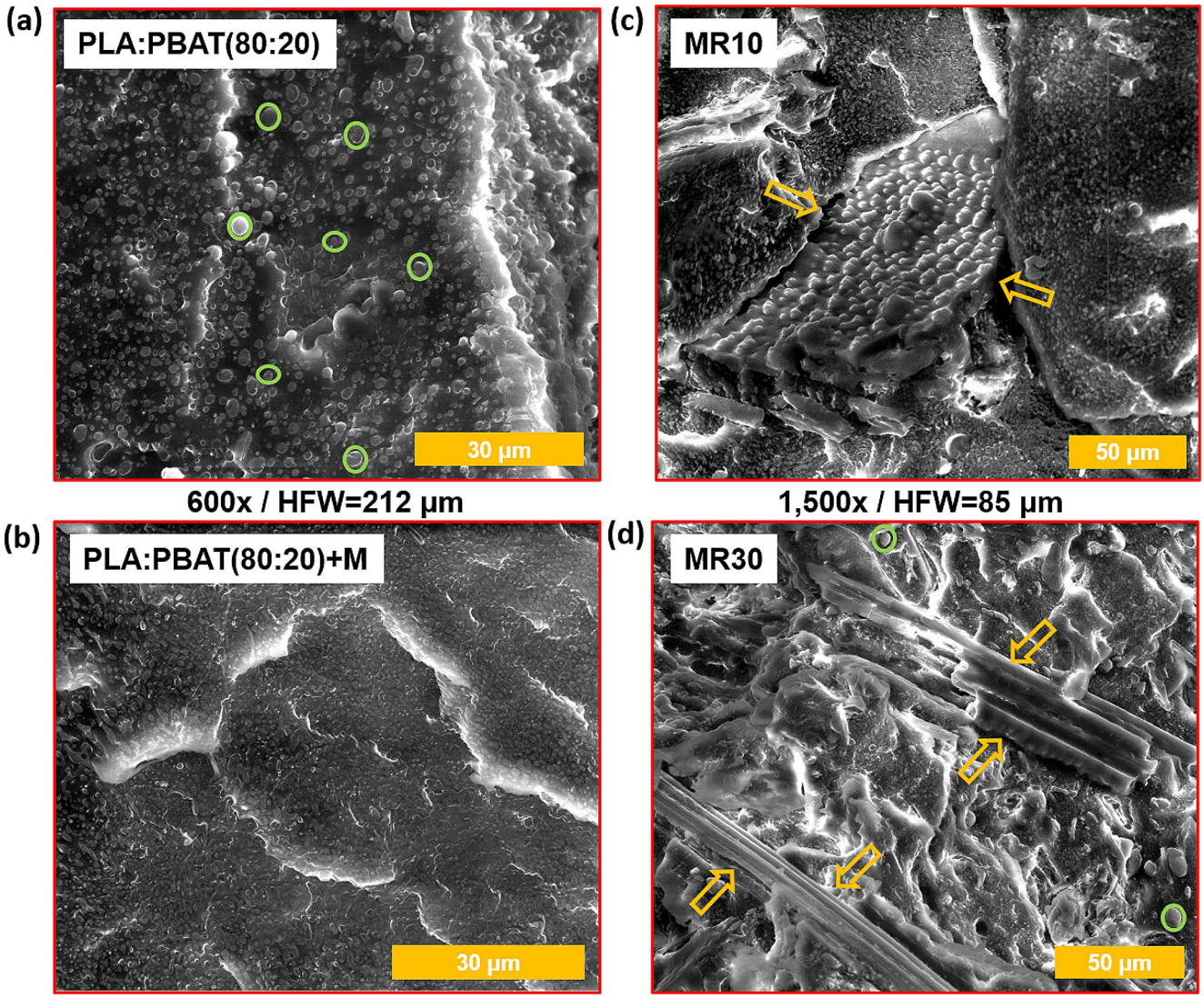

Fig. 6 SEM micrograms of the MA containing specimens at 600 and 1,500x magnifications. (**a**) baseline blend of PLA: PBAT (80:20); (**b**) compatibilized blend with 5 wt% MA; (**c**) MA compatibilized composite with 10 wt% rice straw microparticles; and (**d**) MA compatibilized composite with 30 wt% rice straw microparticles

between the blend systems and the rice straw particles (see orange arrows in SEMs). This results in enhanced disruption between the particles themselves. Additionally, the matrix exhibits a more homogenized morphology, confirming that the rice straw particles remain below 250 µm in size without clustering or undergoing agglomeration due to poor bonding interactions. When comparing the performance of the compatibilizing agents within the composite systems, the *Joncryl*® additive stands out for its effectiveness. In Fig. 5(c) and (d), it is evident that the particles exhibit greater polymer coverage and improved wetting, making it challenging to discern the particle edges, even at higher filler levels. In contrast, the MA compatibilized systems exhibit a clearer interfacial boundary layer between the matrix and composite material, along with less effective wetting of the actual particles, as illustrated in Fig. 6(c) and (d). This improved dispersion and bonding have significant implications for properties such as tensile strength and fracture toughness, as they lead to enhanced stress transfer in the material.

When blending two polymers, it is expected to obtain tensile strength and modulus values falling between those of the baseline values of the individual constituents. However, when the matrix is not compatible, the resulting mechanical properties may deteriorate due to poor stress transfer. Upon examining the tensile strength of the blend and the compatibilized blend in Fig. 7(a), there is a slight increase in both cases. However, these increases are not statistically significant, as they fall within the range of the standard deviation of the baseline blend's values. This outcome can be attributed to the secondary phase (e.g., PBAT) being

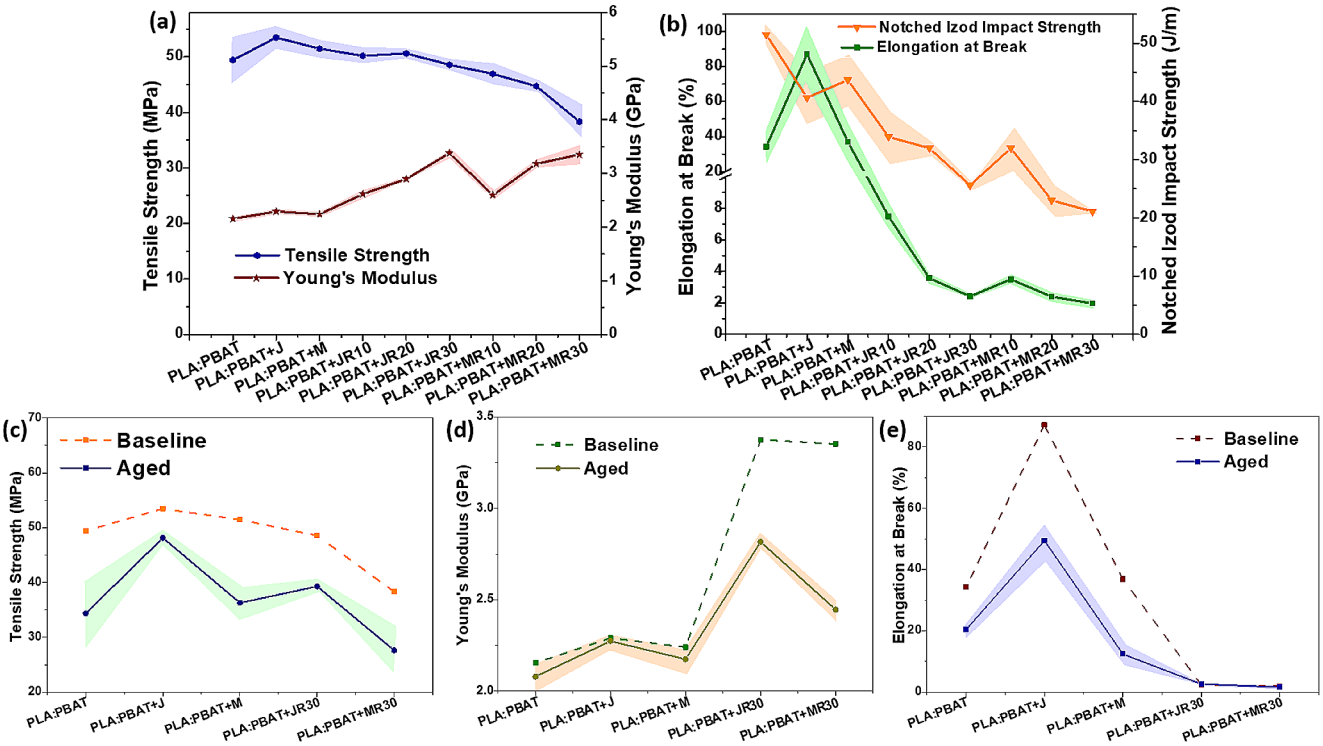

Fig. 7 (**a**) tensile strength and modulus of the blends and rice straw composites; (**b**) elongation at break and notched izod impact results of the blends and composites; (**c**) Aged comparison. Shaded background shows standard deviation

Table 2 Zero shear viscosity data was obtained before and after weathering trials and curves fitted with the *Cross* model

Specimen code	Zero-shear viscosity (Pa·s) (before aging)	R^2	Zero-shear viscosity (Pa·s) (after aging)	R^2
PLA: PBAT	1.25×10^4	0.9949	2.58×10^3	0.9941
PLA: PBAT + M	2.02×10^4	0.9873	88.0	0.9504
PLA: PBAT + J	1.62×10^5	0.9978	1.24×10^4	0.9995
MR10	8.85×10^3	0.9922	/	/
MR20	1.16×10^4	0.9932	/	/
MR30	6.42×10^4	0.9980	1.69×10^5	0.9999
JR10	7.23×10^4	0.9947	/	/
JR20	1.77×10^6	0.9992	/	/
JR30	3.46×10^7	0.9952	2.60×10^4	0.9840

well-dispersed and only making a minor contribution to the PLA's matrix, as confirmed in the micrographic images of the blends shown in Fig. 5. Please note that the shaded areas around the trend line represent the standard deviation of the samples.

In the case of the composites with *Joncryl*®, there is a slight decrease in tensile strength (approximately 8%), as shown in Fig. 7(a). This decrease can be attributed to the rice straw acting as a minor impurity. Nevertheless, the drop in tensile strength is minimal due to the effective dispersion of the rice straw particles and compatibility between all components. It's worth noting that the addition of higher levels of rice straw does not significantly affect the tensile strength until reaching 30 wt%, at which point there is a more pronounced drop of approximately 10%, matching the tensile strength of the baseline blend.

The maleated composites, on the other hand, exhibit a notable and consistent decrease in tensile strength starting as early as 10 wt% with an 8% decline, worsening to a ~ 26% reduction at 30 wt% from Fig. 7(a). This decline in properties is likely the result of a combination effect. The presence of DCP could lead to excessive chain scission [38], and maleic anhydride (MA) could also be less effective at achieving compatibility among all components simultaneously [39]. Since MA is introduced at the beginning, the carbonyl groups may focus more on the PLA and PBAT, reducing stress transfer capabilities. This is reflected in the SEM micrographs, which reveal slight interfacial voids between the matrix and particles (Fig. 6).

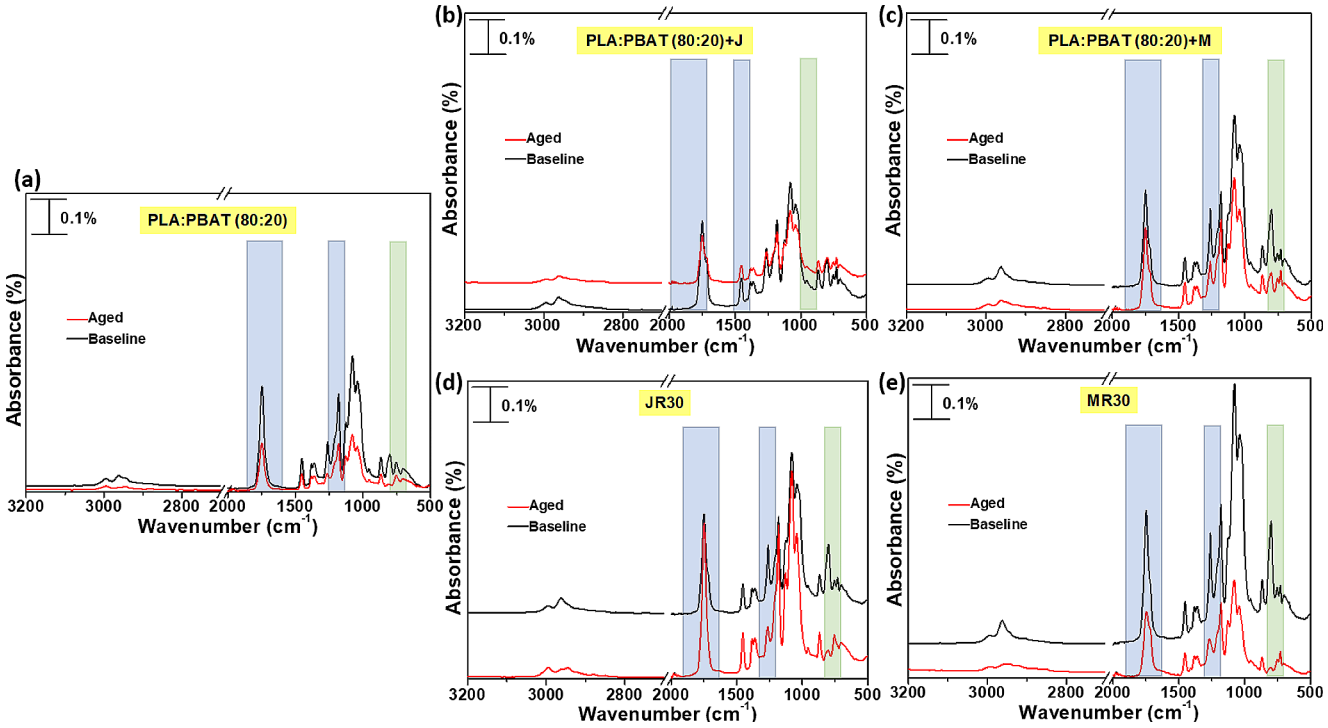

Fig. 8 ATR-FTIR spectra (500 to 3200 cm^{-1}) for comparing the before and after 500 h of cyclic UV and humidity exposure (**a**) PLA: PBAT (80:20); (**b**) PLA: PBAT (80:20) + J; (**c**) PLA: PBAT (80:20) + M; (**d**) JR30; and (**e**) MR30

In contrast to tensile strength, Young's modulus (see Fig. 7(a)) increases with compatibilization due to the increased molecular weight (MW) resulting from crosslinking and branching of the polymer's main chains [40, 41]. In both MA and J composites, Young's modulus demonstrates a gradual rise with each successive addition of rice straw. Notably, the JR30 and MR30 composites exhibit substantial increases, with a 48% rise (from 2.3 to 3.4 GPa) and a remarkable 55% increase (from 2.2 to 3.4 GPa), respectively. This boost in Young's modulus is attributed to the stiffness of the filler compared to the matrix, as well as the effective dispersion of the rice straw particles, facilitated by their small size and partial system compatibilization, which enables some degree of stress transfer between the filler and matrix (Fig. 6).

Elongation at break and notch Izod impact strength (see Fig. 7(b)) both follow a similar trend in the compatibilized blends, with improved ductility properties. Chain extender compatibilized blends experience a more significant improvement due to the higher MW added to the matrix. However, following the addition of rice straw microparticles, both elongation and impact properties decrease significantly. This decline is a result of the restricted chain mobility caused by the presence of particulate reinforcement in the system. Notably, the JR10 system exhibits the highest elongation at break value, owing to the good dispersion of the rice straw, which has a less inhibiting effect on chain mobility.

Accelerated Weathering

Concerning the chemical changes resulting from weathering (see Fig. 8(a) to (e)), one of the most prominent alterations observed in the ATR-FTIR spectra, particularly for the baseline and composites, is the disappearance of a strongly intense peak at 802 cm^{-1} (green column on the graphs). This peak is likely associated with PBAT's aromatic component [42]. It's plausible that the benzene ring undergoes transformations into phenyl or acyl type radicals, contributing to the formation of additional groups such as substituted benzenes, fulvene, or benzophenone structures, which represent the insoluble fraction of the polymer group [43–45]. Therefore, the absence of benzophenone-like tri-substituted phenyls suggests a loss of the 3D network (i.e., crosslinking) or, at the very least, the radicalization and opening of the aromatic ring on PBAT's main chain after weathering.

In contrast, the disappearance of this peak doesn't occur in the compatibilized system, although its intensity decreases. This implies that both compatibilizers are effective at maintaining the newly formed structural architecture of the system (i.e., crosslinking). Supporting evidence for this peak assignment comes from the medium-intensity peaks on either side of it, which are associated with the

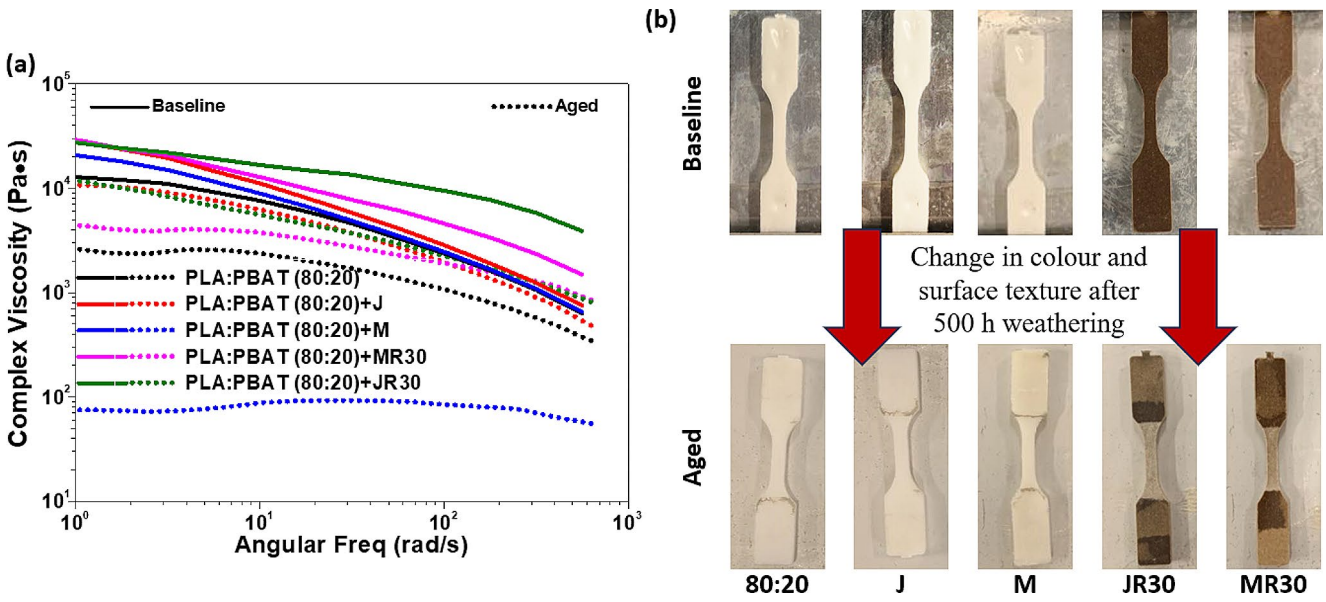

Fig. 9 (**a**) Complex viscosity comparison of before and after 500 h of cyclic UV radiation and humidity exposure as well as (**b**) show photos capturing the physical changes that occurred after aging

-C-C- stretching of the amorphous (867 cm^{-1}) and crystalline (752 cm^{-1}) phases, in addition to the out-of-plane ring deformation from PBAT at 750 cm^{-1} [42, 43, 46]. Lastly, the regions at 1261 and 1751 cm^{-1}, corresponding to -C-O- ester and C = O carbonyl groups (blue columns Fig. 7), also exhibit noticeable reductions in their respective peak intensities. These reductions can be attributed to ester bond cleavage, resulting in a decrease in molecular weight [42, 43].

With confirmation from ATR-FTIR indicating that chain scission had indeed occurred, a further investigation into the sample's complex viscosity was conducted to quantify the extent of property reduction after artificial aging. As depicted in Fig. 9(a), the complex viscosity decreased for all samples, with the most substantial reduction observed in the maleated blend. In contrast, the composites displayed a less severe drop in complex viscosity. Additionally, the shape of the maleated sample's curve was transformed, exhibiting a Newtonian plateau across virtually the entire frequency sweep and extending into the very high-frequency region. On the other hand, the baseline blend and the chain extender containing sample maintained their overall curve shapes as seen prior to weathering, albeit at reduced complex viscosities. The composites continued to exhibit a characteristic curve resembling that of a power-law fluid. The overall decrease in complex viscosity across all samples can be attributed to molecular fragmentation [46].

As a result of chain scission in the blends, their original glossy white appearance has transformed into a matte texture, which is a typical photodegradation outcome for PLA when exposed to UV radiation (see Fig. 9(b)). This color change arises from PLA-containing chromophore groups, including carbonyls, which actively absorb UV frequencies, initiating the Norrish type II degradation pathway [42]. Additionally, the PBAT compounds experience a change in color as they undergo hydroxylation on the terephthalic ring [42]. In the case of the composites, it's worth noting that for wood plastic composite (WPC) materials and products that have undergone UV degradation the polymer chains will disentangle, through chain scission, which allows the shorter chains to migrate to the composite's surface resulting in the lightening of the sample [47–49]. As well, when WF is exposed to UV rays, photobleaching occurs due to an increase in production of hydroquinone molecules [47–49].

The impact of accelerated weathering on the samples was also investigated by evaluating the change in the tensile properties and molecular structure using infrared spectroscopy. Regarding tensile strength (refer to Fig. 7), all samples experienced a reduction after weathering, with the baseline blend showing the most significant deterioration, exhibiting a 30% decrease (equivalent to 34 MPa). Following closely were the MA-containing blend and composite, both experiencing a 29% reduction (36 MPa) and a 27% decrease (27 MPa), respectively. In contrast, the chain extender containing blend and composite demonstrated the highest tensile strength retention, with reductions of 10% and 19%, respectively. This resilience can be attributed to the decrease in molecular weight (MW) resulting from weathering, as both PBAT and PLA contain photosensitive groups, including benzenes and carbonyls [35, 42, 43, 46]. Furthermore, PLA is photosensitive, following the Norrish type II photolysis mechanism [26]. In both cases, the decrease in MW

adversely affects the mechanical properties of the system, leading to a loss of crystallinity and modulus, while also causing changes in color and texture (see Fig. 9(b)) [35, 46].

Interestingly, chain extender samples exhibited less property deterioration compared to the baseline blend, primarily because the *Joncryl*® systems possesses a higher degree of crosslinking between adjacent polymer chains and filler particles. This enhanced crosslinking contributes to greater durability, particularly for applications exposed to external environmental factors [35]. Notably, it's intriguing to observe that the composites experienced similar or even higher property losses compared to the blends. This phenomenon is likely attributed to humidity, as the biomass fillers and resulting composites have the propensity to gradually absorb moisture over time that leads to property deterioration. The higher degree of crosslinking within the *Joncryl*® composite enabled it to retain more tensile strength when compared to the maleated composite [35]. This suggests that chain extender has greater potential for compatibility by reducing interfacial voids within the composite, thereby inhibiting water absorption mechanisms, including diffusivity, permeability, and sorption, to a greater extent than the maleated compatibilizing agent. In contrast, the blends are less affected by humidity because the primary phase, PLA, is known for its resistance to active moisture absorption or breakdown when exposed to water or humid environments [46].

The same pattern is evident in the tensile modulus (Fig. 7(b)) where the *Joncryl*® samples exhibit higher property retention compared to all other samples after 500 h of weathering. Nonetheless, the reduction in modulus across all samples can also be attributed to the softening of the rice filler as moisture slowly permeates it, leading to a decrease in the biomass's stiffness, coupled with molecular fragmentation of the polymers [50]. When a 40 wt% rice straw filler is present, achieving complete coverage or wetting of the particles by the matrix becomes more challenging, making it difficult to shield them entirely from moisture, exacerbated by their inherent poor compatibility with the matrix. Lastly, the elongation at break (Fig. 7(c)) follows a similar trend as the tensile strength and modulus. However, the loss in % strain is minimal in the composites before and after weathering. This is primarily due to the synergistic effect of PLA being inherently brittle, combined with the presence of a rigid filler at 40 wt%, which limits the overall strain capacity of the material.

Conclusions

Through the blending and compatibilization of PLA and PBAT utilizing two different compatibilizers, it was determined that the Joncryl based-chain extender (J) outperformed maleic anhydride (MA) in facilitating a higher degree of crosslinking and compatibilization (6% from gel-fractionation) between the two polymers as well as with the rice filler (~21% gel content). The *Joncryl*® was determined to be the superior additive based on the blend's and composite's higher viscosity ($\sim 2 \times 10^4$ Pa•s for MA vs. $\sim 2 \times 10^5$ Pa•s for J) and enhanced tensile strength (51 to 54 MPa for MA and J blends, respectively), indicating better interaction. Moreover, SEM analysis illustrated the effectiveness of these compatibilizing agents by transforming the initial two-phase morphology into a homogenized morphology within the blends while also reducing interfacial voids in the composite systems. Upon the addition of rice straw, a decrease in the tensile strength of the system was observed due to the overall poor compatibility between rice straw and the blended matrix. However, the modulus experienced a significant increase (2.2 GPa from the blend to 3.4 GPa for the R30 samples), due to the well-dispersed micro-sized rice straw particles. Notably, the rice straw particles had a notable nucleating effect on the T_G of the PLA phase within the blend, causing the T_G to shift to lower temperatures (70 to 65 °C). Additionally, the inclusion of rice straw contributed to increased composite viscosity, which further escalated with the addition of well-dispersed rice straw microparticles.

Following exposure to weathering, all samples exhibited property degradation in terms of tensile properties (10–19% reduction for J vs. 27–30% for MA), viscosity (with a maximum of $\sim 3 \times 10^7$ Pa•s for the JR30 sample), and aesthetics. Nevertheless, the chain extender treated samples retained the highest number of properties due to their more pronounced degree of crosslinking when compared to those treated with MA.

Supplementary Information The online version contains supplementary material available at https://doi.org/10.1007/s10924-024-03314-5.

Acknowledgements This work was achieved due to the financial support of KENTECH who also graciously supplied of rice straw biomass in an unrefined form. The PLA resin used in this study was graciously donated by Total Energies Corbion.

Author Contributions Dylan Jubinville (DJ): Procedure, research, formal investigation, writing, review & editing. Mohammed Awad (MA): Procedure, research, formal investigation, writing, review & editing. Hyungsool Chris Lee (HS): Conceptualization, project management, administration, editing. Tizazu H. Mekonnen (TM): Conceptualization, project management, administration, editing. All authors read and approved the final manuscript.

Data Availability No datasets were generated or analysed during the current study.

Declarations

Competing Interests The authors declare no competing interests.

References

1. Shirley M (2022) Rice. Food and Agriculture Organization of the United Nations (FAO)
2. Jin S, Chen H (2007) Near-infrared analysis of the chemical composition of rice straw. Ind Crops Prod 26:207–211. https://doi.org/10.1016/j.indcrop.2007.03.004
3. Yao F, Wu Q, Lei Y, Xu Y (2008) Rice straw fiber-reinforced high-density polyethylene composite: Effect of fiber type and loading. Ind Crops Prod 28:63–72. https://doi.org/10.1016/j.indcrop.2008.01.007
4. Matías J, Cruz V, García A, González D (2019) Evaluation of Rice Straw Yield, Fibre Composition and Collection under Mediterranean conditions. Acta Technologica Agriculturae 22:43–47. https://doi.org/10.2478/ata-2019-0008
5. Smith PA, Yeomans JA (2009) Benefits of Fibre and Particulate reinforcements. In: Rawlings R (ed) Materials Science and Engineering. Encyclopedia of Life Support Systems, Oxford, pp 133–141
6. Xia T, Huang H, Wu G et al (2018) The characteristic changes of rice straw fibers in anaerobic digestion and its effect on rice straw-reinforced composites. Ind Crops Prod 121:73–79. https://doi.org/10.1016/j.indcrop.2018.04.004
7. Sun Y, Zheng Z, Wang Y et al (2022) PLA composites reinforced with rice residues or glass fiber—a review of mechanical properties, thermal properties, and biodegradation properties. J Polym Res 29:422. https://doi.org/10.1007/s10965-022-03274-1
8. Beniwal P, Toor AP (2023) Advancement in tensile properties of polylactic acid composites reinforced with rice straw fibers. Ind Crops Prod 192:116098. https://doi.org/10.1016/j.indcrop.2022.116098
9. Qin L, Qiu J, Liu M et al (2011) Mechanical and thermal properties of poly(lactic acid) composites with rice straw fiber modified by poly(butyl acrylate). Chem Eng J 166:772–778. https://doi.org/10.1016/j.cej.2010.11.039
10. Grozdanov A, Buzarovska A, Bogoeva-Gaceva G et al (2006) Rice straw as an alternative reinforcement in polypropylene composites. Agron Sustain Dev 26:251–255. https://doi.org/10.1051/agro:2006023
11. Dinh Vu N, Thi Tran H, Duy Nguyen T (2018) Characterization of Polypropylene Green composites Reinforced by Cellulose fibers extracted from Rice Straw. Int J Polym Sci 2018:1–10. https://doi.org/10.1155/2018/1813847
12. Ashori A (2013) Effects of nanoparticles on the mechanical properties of rice straw/polypropylene composites. J Compos Mater 47:149–154. https://doi.org/10.1177/0021998312437234
13. Arruda LC, Magaton M, Bretas RES, Ueki MM (2015) Influence of chain extender on mechanical, thermal and morphological properties of blown films of PLA/PBAT blends. Polym Test 43:27–37. https://doi.org/10.1016/j.polymertesting.2015.02.005
14. Palsikowski PA, Kuchnier CN, Pinheiro IF, Morales AR (2018) Biodegradation in Soil of PLA/PBAT blends compatibilized with Chain Extender. J Polym Environ 26:330–341. https://doi.org/10.1007/s10924-017-0951-3
15. Jubinville D, Tzoganakis C, Mekonnen TH (2022) Recycled PLA–Wood flour based biocomposites: Effect of wood flour surface modification, PLA recycling, and maleation. Constr Build Mater 352:129026. https://doi.org/10.1016/j.conbuildmat.2022.129026
16. Ceraulo M, La Mantia FP, Mistretta MC, Titone V (2022) The Use of Waste Hazelnut shells as a reinforcement in the development of Green biocomposites. Polym (Basel) 14:2151. https://doi.org/10.3390/polym14112151
17. Botta L, Titone V, Mistretta MC et al (2021) PBAT Based composites Reinforced with Microcrystalline Cellulose Obtained from Softwood Almond shells. Polym (Basel) 13:2643. https://doi.org/10.3390/polym13162643
18. Lima EMB, Middea A, Neumann R et al (2021) Biocomposites of PLA and Mango seed Waste: potential material for Food Packaging and a Technological Alternative to Reduce Environmental Impact. Starch - Stärke 73:. https://doi.org/10.1002/star.202000118
19. Seldén R, Nyström B, Långström R (2004) UV aging of poly(propylene)/wood-fiber composites. Polym Compos 25:543–553. https://doi.org/10.1002/pc.20048
20. International Standard (2006) ISO 4892-3: Plastics — methods of exposure to laboratory light sources — part, vol 3. Fluorescent UV lamps
21. Dzul-Cervantes M, Herrera-Franco PJ, Tábi T, Valadez-Gonzalez A (2017) Using Factorial Design Methodology to assess PLA-g-Ma and Henequen Microfibrillated Cellulose Content on the Mechanical properties of Poly(lactic acid) composites. Int J Polym Sci 2017. https://doi.org/10.1155/2017/4046862
22. Thiyagu TT, J.V SPK PG et al (2021) Effect of cashew shell biomass synthesized cardanol oil green compatibilizer on flexibility, barrier, thermal, and wettability of PLA/PBAT biocomposite films. Biomass Convers Biorefin. https://doi.org/10.1007/s13399-021-01941-9
23. Kijchavengkul T, Auras R, Rubino M (2008) Measuring gel content of aromatic polyesters using FTIR spectrophotometry and DSC. Polym Test 27:55–60. https://doi.org/10.1016/j.polymertesting.2007.08.007
24. Kumar M, Mohanty S, Nayak SK, Rahail Parvaiz M (2010) Effect of glycidyl methacrylate (GMA) on the thermal, mechanical and morphological property of biodegradable PLA/PBAT blend and its nanocomposites. Bioresour Technol 101:8406–8415. https://doi.org/10.1016/j.biortech.2010.05.075
25. Wu C-S (2009) Renewable resource-based composites of recycled natural fibers and maleated polylactide bioplastic: characterization and biodegradability. Polym Degrad Stab 94:1076–1084. https://doi.org/10.1016/j.polymdegradstab.2009.04.002
26. Sakhiya AK, Anand A, Vijay VK, Kaushal P (2021) Thermal decomposition of rice straw from rice basin of India to improve energy-pollution nexus: kinetic modeling and thermodynamic analysis. Energy Nexus 4:100026. https://doi.org/10.1016/j.nexus.2021.100026
27. Yulidar Y, Saiful S, Maulana I (2019) Purification of Biodiesel using Rice Straw and Dioscorea Alata Starch as Natural adsorbents. Jurnal Nat 19:12–17. https://doi.org/10.24815/jn.v19i1.12452
28. Bee S-T, Ratnam CT, Sin LT et al (2014) Effects of electron beam irradiation on the structural properties of polylactic acid/polyethylene blends. Nucl Instrum Methods Phys Res B 334:18–27. https://doi.org/10.1016/j.nimb.2014.04.024
29. Gupta A, Chudasama B, Chang BP, Mekonnen T (2021) Robust and sustainable PBAT– hemp residue biocomposites: reactive extrusion compatibilization and fabrication. Compos Sci Technol 215:109014. https://doi.org/10.1016/j.compscitech.2021.109014
30. Zhang Y, Jia S, Pan H et al (2021) Effect of glycidyl methacrylate-grafted poly(ethylene octene) on the compatibility in PLA/PBAT blends and films. Korean J Chem Eng 38:1746–1755. https://doi.org/10.1007/s11814-021-0809-1

31. Wu N, Zhang H (2017) Mechanical properties and phase morphology of super-tough PLA/PBAT/EMA-GMA multicomponent blends. Mater Lett 192:17–20. https://doi.org/10.1016/j.matlet.2017.01.063
32. Borysiak S (2007) Determination of nucleating ability of wood for non-isothermal crystallization of polypropylene. J Therm Anal Calorim 88:455–462. https://doi.org/10.1007/s10973-006-8077-1
33. Rosa SML, Nachtigall SMB, Ferreira CA (2009) Thermal and dynamic-mechanical characterization of rice-husk filled polypropylene composites. Macromol Res 17:8–13. https://doi.org/10.1007/BF03218594
34. Fuad MYA, Mustafah J, Mansor MS et al (1995) Thermal properties of polypropylene/rice husk ash composites. Polym Int 38:33–43. https://doi.org/10.1002/pi.1995.210380104
35. Tang D, Zhang C, Weng Y (2021) Effect of multi-functional epoxy chain extender on the weathering resistance performance of poly(butylene adipate-co-terephthalate) (PBAT). Polym Test 99:107204. https://doi.org/10.1016/j.polymertesting.2021.107204
36. Al-Itry R, Lamnawar K, Maazouz A (2012) Improvement of thermal stability, rheological and mechanical properties of PLA, PBAT and their blends by reactive extrusion with functionalized epoxy. Polym Degrad Stab 97:1898–1914. https://doi.org/10.1016/j.polymdegradstab.2012.06.028
37. Chen W, Qi C, Li Y, Tao H (2021) The degradation investigation of biodegradable PLA/PBAT blend: thermal stability, mechanical properties and PALS analysis. Radiat Phys Chem 180:109239. https://doi.org/10.1016/j.radphyschem.2020.109239
38. Wang D, Xu W, Sun G, Chiou B (2011) Radical graft polymerization of an Allyl Monomer onto Hydrophilic polymers and their antibacterial nanofibrous membranes. ACS Appl Mater Interfaces 3:2838–2844. https://doi.org/10.1021/am200286a
39. Seguchi T, Arakawa K, Hayakawa N et al (1982) Radiation induced oxidative degradation of polymers—II. Radiation Phys Chem (1977) 19:321–327. https://doi.org/10.1016/0146-5724(82)90116-9
40. Mo Z, Liu X, Liu Y et al (2023) Effect of styrene-maleic anhydride on phase morphology and properties of PLA/PBAT blends. Fuhe Cailiao Xuebao/Acta Materiae Compositae Sinica 40:2096–2106. https://doi.org/10.13801/j.cnki.fhclxb.20220630.001
41. Al-Itry R, Lamnawar K, Maazouz A et al (2015) Effect of the simultaneous biaxial stretching on the structural and mechanical properties of PLA, PBAT and their blends at rubbery state. Eur Polym J 68:288–301. https://doi.org/10.1016/j.eurpolymj.2015.05.001
42. Scaffaro R, Maio A, Gammino M, La Mantia FP (2021) Effect of an organoclay on the photochemical transformations of a PBAT/PLA blend and morpho-chemical features of crosslinked networks. Polym Degrad Stab 187:109549. https://doi.org/10.1016/j.polymdegradstab.2021.109549
43. Yang Y, Zhang C, Weng Y (2021) Effects of CaCO3 surface modification and water spraying on the weathering properties of PBAT/CaCO3 films. Polym Test 102:107334. https://doi.org/10.1016/j.polymertesting.2021.107334
44. Mouzay J, Piétri N, Couturier-Tamburelli I, Chiavassa T (2021) UV irradiation of benzene in N2 matrix: a relevant study for Titan's chemistry. J Mol Struct 1237:130296. https://doi.org/10.1016/j.molstruc.2021.130296
45. Bathla A, Vikrant K, Kukkar D, Kim K-H (2022) Photocatalytic degradation of gaseous benzene using metal oxide nanocomposites. Adv Colloid Interface Sci 305:102696. https://doi.org/10.1016/j.cis.2022.102696
46. González-López ME, del Martín AS, Robledo-Ortíz JR et al (2020) Accelerated weathering of poly(lactic acid) and its biocomposites: a review. Polym Degrad Stab 179:109290. https://doi.org/10.1016/j.polymdegradstab.2020.109290
47. Du H, Wang W, Wang Q et al (2010) Effects of pigments on the UV degradation of wood-flour/HDPE composites. J Appl Polym Sci 118:n/a-n/a. https://doi.org/10.1002/app.32430
48. Xing Q, Ruch D, Dubois P et al (2017) Biodegradable and high-performance poly(butylene adipate-co-terephthalate)–Lignin UV-Blocking films. ACS Sustain Chem Eng 5:10342–10351. https://doi.org/10.1021/acssuschemeng.7b02370
49. Botta L, Titone V, Teresi R et al (2022) Biocomposite PBAT/lignin blown films with enhanced photo-stability. Int J Biol Macromol 217:161–170. https://doi.org/10.1016/j.ijbiomac.2022.07.048
50. Mekonnen T, Mussone P, Alemaskin K et al (2013) Biocomposites from hydrolyzed waste proteinaceous biomass: mechanical, thermal and moisture absorption performances. J Mater Chem Mater 1:13186–13196. https://doi.org/10.1039/c3ta13560h